LA-UR - 74-738

Conf-740320--3

TITLE: MODELS BASED ON MULTICHANNEL R-MATRIX THEORY FOR EVALUATING LIGHT ELEMENT REACTIONS

AUTHOR(S): D. C. Dodder, G. M. Hale, R. A. Nisley, K. Witte, and P. G. Young

SUBMITTED TO: Proceedings, EANDC Topical Discussion on Critiques of Nuclear Models and Their Validity in the Evaluation of Nuclear Data" in Tokyo, March 28, 1974.

los alamos
scientific laboratory
of the University of California
LOS ALAMOS, NEW MEXICO 87544

Form No. 836
St. No. 2629
1/73

UNITED STATES
ATOMIC ENERGY COMMISSION
CONTRACT W-7405-ENG. 36

Models Based on Multichannel R-Matrix Theory for Evaluating Light Element Reactions*

D. C. Dodder, G. M. Hale, R. A. Nisley, K. Witte, and P. G. Young

Los Alamos Scientific Laboratory, University of California

Los Alamos, New Mexico 87544

Abstract

Multichannel R-matrix theory has been used as a basis for models for analysis and evaluation of light nuclear systems. These models have the characteristic that data predictions can be made utilizing information derived from other reactions related to the one of primary interest. Several examples are given where such an approach is valid and appropriate.

---

* Work performed under the auspices of the United States Atomic Energy Commission.

Models Based on Multichannel R-Matrix Theory for Evaluating Light Element Reactions

D. C. Dodder, G. M. Hale, R. A. Nisley, K. Witte, and P. G. Young

As has no doubt been emphasized in the other papers in this symposium, the reason for using models in data evaluations is to try to make use of more information than is just contained in the measurements under consideration. This additional information ranges all the way from knowledge of the general laws of nature to results of explicit measurements closely related to those being evaluated. In the same way models range, in their philosophy, from little more than mathematical parameterizations of data to detailed and realistic constructs clearly based on our knowledge of physics. We would like to show that the R-matrix formalism of Wigner and Eisenbud[1] offers a framework for embodying a number of different model concepts in nuclear data evaluation.

The R-matrix theory is a general formalism that is really a method of description that insures compatability with fundamental physical laws. Invariance principles such as unitarity and conservation of total angular momentum are maintained, and in addition it can be shown that its content is closely related to requirements of causality. Within this framework it is an economical and appropriate description for many observed phenomena. In its most general form it is already a model in the sense that it does insist on compliance with the general laws involved in its derivation; on the other hand much more model-like behavior can be imposed by constraining the values of its parameters in appropriate ways. We shall give a number of examples of this.

Even an outline of the derivation of R-matrix theory[2] is beyond the scope of this report. Some idea of its structure however is essential to understanding our point of view. The entire observational content of collision processes is contained in the so-called collision matrix (S-matrix). This matrix, relying on the superposition principle of quantum mechanics, essentially gives the outgoing amplitudes of a collision in terms of the incoming ones. At this descriptive level of procedure certain general symmetry principles are directly reflected in the structure of the collision matrix. The conservation of particles is imposed by having the matrix unitary. Time reversal invariance is equivalent to having the matrix symmetric in a suitable representation. And finally conservation of total angular momentum and parity means that the matrix can be so chosen as to reduce to a series of disconnected submatrices along the diagonal, each submatrix referring to a state of given J and parity and each submatrix being individually unitary and symmetric.
It is evident that already a description of scattering and reaction processes at this level demands relationships between the different processes and that the requirement of consistency is a valuable aid to data evaluation.

The energy dependence of the collision matrix elements is, however, quite complicated, and depends on the external Coulomb and centrifugal barriers as well as the nuclear forces. This is seen even in the simple case of a single isolated energy level, where the cross section for a transition from state i to state f is given by:

$$\sigma_{fi} \simeq \frac{\Gamma_i \Gamma_f}{(E - E_r)^2 + \frac{1}{4}(\Gamma_i + \Gamma_f)^2}$$

Here the widths Γ_i and Γ_f have factors (the so-called penetration factors) which are often strongly energy dependent, and the resonant energy E_r is also in general energy dependent. The R-matrix formalism deals with this situation by dividing the configuration space in each channel into an inner and an outer region, the inner region being that where the strong interaction predominates, and the outer that where only the Coulomb force exists, and where the main effect of the centrifugal barrier is felt. The R-matrix itself is a relationship between the values and derivatives of the wave functions at the boundary between the two regions. The theory shows that the R-matrix must, under very general assumptions about the nature of the interaction in the inner region, have the form

$$R^J_{\alpha's'\ell',\alpha s\ell} = \sum_\lambda \frac{\gamma^J_{\lambda\alpha s\ell}\ \gamma^J_{\lambda\ \alpha's'\ell'}}{E^J_\lambda - E}$$

where J, s, ℓ have their usual meanings, α is the channel label, E is the C.M. energy, E^J_λ are the eigenvalues of the Hamiltonian operator in the interior region with a certain set of boundary conditions on the logarithmic derivatives of the wave functions, and the $\gamma_{\lambda\alpha s\ell}$, the reduced width amplitudes, are essentially the values of the wave functions on the boundaries. The collision matrix can be expressed in terms of the R-matrix but we shall not give the expression here. We usually let the computing machine do this rather tedious work. The point is that the rather simple form of the R-matrix allows model-like behavior to be used in parameterization of the nuclear data. And the main reason this is appropriate is that the values of radii in the different channels which are the boundaries between the inner

and outer regions, correspond in a real way to the actual nuclear radii in the different configurations. This means that the physically occurring cutoff in ℓ values is naturally accounted for in R-matrix calculations through the dependence of the phase shifts on the penetration factors.

In the employment of the R-matrix approach as a model it is clear that it will be macroscopic like the optical model, rather than microscopic like the shell model. Its usefulness is indicated by a few general observations. The levels and widths occurring in the general R-matrix expression can be made to correspond to real energy levels of physical systems and frequently relatively few suffice to entirely describe a given (J^π parity) state. Furthermore, symmetries of the internal Hamiltonian can be applied directly to the R-matrix. In cases where the internal interaction is dominated by nuclear forces, for instance, it is appropriate to impose constraints reflecting parity conservation and charge symmetry or charge independence (isospin conservation) on the R-matrix parameters.

The application of such an R-matrix model to the elastic scattering of nucleons from ^{4}He has been highly successful. Almost all available measurements for p-α and n-α scattering at lab energies in the 0-20 MeV range were analyzed simultaneously, with R-matrix parameters in the two systems related by a simple model of the charge symmetry. Specifically, for common boundary conditions imposed at the same channel radius, the reduced width amplitudes for a given level were constrained to be equal ($\gamma_{\lambda p} = \gamma_{\lambda n}$), and the level energies were constrained to differ by a Coulomb

"shift" ΔE ($E_{\lambda p} = E_{\lambda n} + \Delta E$) that was taken to be the same for all levels. In addition to the known p-wave levels, distant-level contributions were represented in each state by single pole terms. Partial waves having $\ell > 3$ were neglected. Thus constrained and truncated, the combined R-matrix analysis required 15 free parameters, just one parameter (ΔE) more than the number needed to analyze either p-α or n-α scattering separately.

Figure 1[3] shows the resulting least squares fit (solid line)* to a segment of the n-α total cross section over the 1.25 MeV resonance (the dotted curve is ENDF/B III). Figures 2-4 show representative fits to the n-α differential cross sections, while Figs. 5 and 6 show representative fits to the n-α analyzing powers (or polarizations) over the energy range considered. On Fig. 7 is given a sampling of the fits to the p-α differential cross sections, and Fig. 8 shows fits to various p-α polarization measurements. Note that the top two curves in the right column of Fig. 8 represent measurements ($K_x^{x'}$, $K_z^{x'}$) of outgoing proton polarization with a polarized proton beam incident. In general, the p-α experiments were more numerous and more precise than the n-α experiments, and we feel that even this simple charge-symmetric model has imposed better accuracy on the predicted n-α observables than can be attained in most present n-α measurements.

Interestingly, the parameters which fit the data indicated that an even more stringent model might have been imposed. The channel radius preferred a value (2.9 f.) close to that expected from the nuclear sizes. The reduced widths of the two p-wave levels became, for the first time

- - - - - - - - - -

* The solid line represents the R-matrix fit on this and all succeeding figures.

in such an analysis, approximately equal to each other and to the single-particle width. The phenomenologically determined Coulomb energy shift (ΔE = 1.58 MeV) agreed well with calculations using realistic ^{4}He charge densities. It is pleasing that the parameters moved naturally toward values characteristic of a very simple mechanism for the elastic scattering of nucleons from ^{4}He, namely, single-particle scattering from a simple potential.

The invariance under charge symmetry shown by the nucleon-^{4}He systems is a manifestation of the more general principle of isospin conservation, and that invariance in the internal region can be applied to the R-matrix parameters. An example is found in the 4-nucleon systems. The p-^{3}He and n-T elastic scatterings occur only in the T = 1 state, while among the pairs of the system of p-T, n-^{3}He, and d-D, the d-D channel is only in the T = 0 state while the other two are in both the T = 0 and T = 1 states. By using R-matrix levels of pure isospin states, and constraining the reduced widths in the various channels to being appropriate Clebsch-Gordan fractions of the isospin widths, it is possible to guarantee exact charge independence in the internal region, while still predicting the isospin mixing in the external region which is caused by the different Coulomb potentials in the different channels.[4] The differences in Coulomb energy among the Z = 1, Z = 2, and Z = 3 systems are still expected to be accounted for mainly by a shift in the E_λ's. Our current analysis is using the T = 1 parameters from the p-^{3}He system in the ^{4}He compound system, but eventually all three systems will be analyzed simultaneously.

Although the major concern of evaluation work has been with cross sections for neutron-induced reactions, we feel it is essential in these analyses to include data of various types and from all important reactions that bear on the compound system in which the neutron-induced reactions occur. Primarily through unitarity, data from other reactions determine the model parameters more accurately, which in turn generate more reliable predictions of the neutron cross sections of interest. The analysis we are doing of reactions in the ^{11}B system among the channels $n-^{10}B$, $\alpha-^{7}Li(g.s.)$, and $\alpha-^{7}Li^{*}(.478)$, is a case in point. The large spin of ^{10}B (spin 3) introduces many scattering amplitudes into the problem even for low partial waves, so that including data from a variety of sources is important.

Examples of the types of data we are fitting in our analysis at low energies ($E_n \leq 1$ MeV) are given in the next few figures. Figure 9 shows the fit to the total neutron cross section for ^{10}B (again, the dotted curve is ENDF III), while Fig. 10 displays the fits to integrated $^{10}B(n,\alpha_o)^{7}Li$ and $^{10}B(n,\alpha_1)^{7}Li^{*}$ cross sections. As you can see in the bottom part of this figure, there are severe disagreements among the experiments, particularly above 100 keV. Fits to the $^{10}B(n,n)^{10}B$ differential cross section and polarization measurements of Lane are shown at two energies on Fig. 11. The experimental values ($\pm$) shown for the polarizations (on the right) may not be accurate, since they were generated from Legendre coefficients, but the change of sign in the polarization is significant, indicating the presence of a p-wave

resonance in this energy region (at ≈ 450 keV). Figure 12 shows examples of the fits to $^{10}B(n,\alpha_o)$ differential cross sections obtained by detailed balance from the recent $^{7}Li(\alpha,n)^{10}B$ measurements of Van der Zwaan and Geiger. And the last figure in this sequence (Fig. 13) shows representative fits to the $^{7}Li(\alpha,\alpha)^{7}Li$ differential cross section measurements of Cusson. These fits, as well as those to the $^{7}Li(\alpha,\alpha)^{7}Li^*$ integrated cross section (not shown) indicate that levels with large widths in the α-channels are as yet unidentified in the ^{11}B system. Although these fits for the neutron-induced reactions on ^{10}B represent the most comprehensive analysis effort made thus far at low energies in this system, we feel that the accuracy of the curves is still limited by insufficient data and incomplete knowledge of the level structure of ^{11}B.

As in the case of ^{10}B, the cross sections for neutron-induced reactions on ^{6}Li are important in applications, and particularly in neutron measurements. Our analysis of reactions in the ^{7}Li system gains additional information from including α-T scattering measurements along with data from the $^{6}Li(n,n)^{6}Li$ and $^{6}Li(n,\alpha)T$ reactions. Figure 14 gives examples of the types of $T(\alpha,\alpha)T$ data that are being fit. The upper left-hand part of the figure indicates that the only existing low-energy differential cross section data, even when renormalized, may be seriously in error at back angles. The curve below that is representative of the generally excellent fit obtained to the angular distributions of Ivanovich, Young and Ohlsen at medium energies. Data on the upper right-hand curve are taken from

excitation functions measured by Spiger and Tombrello at an energy close to the 5/2- resonance above the n-^{6}Li threshold. Below that is shown an example of the fit to double-scattering experiments that measure the outgoing triton polarization.

Attention is focused in the next two figures on the region of the important 5/2- resonance near E_n = 250 keV, mentioned earlier. Figure 15 shows for ^{6}Li(n,n) elastic scattering the integrated cross section across the resonance, and (normalized) angular distribution and polarization approximately at resonance. Notice that the fit lies above the experimental points in the peak of the integrated cross section. On Fig. 16 are shown the total neutron cross section for ^{6}Li (top), and the ^{6}Li(n,α)T integrated cross section across the resonance, along with the ^{6}Li(n,α)T differential cross section approximately at resonance. Although it is difficult to tell from the figure, the calculated total cross section peaks at the currently accepted value (~11.0 barns), while the calculated peak (n,α) cross section lies above that of the recent measurements of Coates, Fort, and Poenitz (~3.0 barns). If one believes the total cross section is best determined, then either or both of the observed integrated cross sections is wrong. There are those who feel strongly that the recent measurements of the (n,α) cross section are correct, and that only the (n,n) cross section is too low. Our analysis including the T(α,α)T data in this region indicates that both integrated cross sections are too low. It is an important question, since the ^{6}Li(n,α) cross section is often used as a "standard". Unfortunately, the Spiger and Tombrello data

are not of sufficient quality firmly to resolve the question, but we feel that accurate charged particle measurements in this region might be more useful in resolving these discrepant observations relative to the (n,α) cross section than another direct measurement.

The examples we have so far given are all actually demonstrations of the detail obtainable with these models in realistic data evaluations. We should mention also an example where the work is of a more exploratory nature, where we are trying at first to gain an understanding of the physics involved. The 5 nucleon systems p-α and d-^{3}He and n-α + d-T afford this example. The systems are quantitatively understood at energies up through the famous 3/2+ resonance that occurs in each at a few hundred keV deuteron energies. Above this energy the systems become very complicated, with the scatterings and reactions dominated by a whole series of overlapping resonances mainly in the even parity states of various spin arrangements which have their spatial configuration mainly in the $\ell = 2$ state between the deuteron and the 3-nucleon particle. The R-matrix formalism is an almost ideal mode of description of this situation, and we have succeeded in fitting a rather formidable collection of experimental results in a rather satisfactory fashion.

In the ^{5}Li system, for instance, there have been 39 different types of observables measured for the reactions among d-^{3}He and p-^{4}He. These include, in addition to the usual differential cross sections and polarizations, measurements made with both first- and second-rank polarized deuteron beams incident on ^{3}He, and with polarized proton beams incident on ^{4}He. In some of the experiments, the polarization of the outgoing

particle has been measured. (Examples of these "polarization transfers" have already been shown for $^4He(p,p)^4He$ on Fig. 8.) In others, both polarized and unpolarized deutron beams have been scattered from polarized ^3He targets.

All these various types of measurements have been included in our analyses of the d-^{3}He, p-^{4}He system. The next two figures show examples of fits to a selection of these, taken from an analysis that extends to E_d = 4 MeV. The first of these displays the four independent analyzing tensors (1 first-rank, 3 second-rank) measured by Koenig, et al. for $^3He(d,d)^3He$ at 4 MeV. The second figure gives examples of the fits to measurements made at various energies for $^3He(d,p)^4He$ with both polarized beams and polarized targets.

The examples we have given demonstrate the versatility of the R-matrix approach to data analysis and evaluation. The chief theoretical limitation, which we have not dwelt upon, is the restriction to two-body final states. This can only be avoided at present in those cases where the multi-body final states can be mocked up by quasi- two-body states. We are indeed using this method in the five nuclear system where we take into account the final state p + ^{4}He* as an approximation for the whole spectrum of p + n + ^{3}He and p + p + T breakup channels. A practical limitation of the approach, is, of course, that computers are only so large, and there definitely are limits to the number of channels, ℓ-values and levels we can consider. This limits the work in its present form to the light nuclei. And finally, just because the method of description

is so comprehensive, it is necessary to have a comprehensive data base before the analysis can be successful. This means many experiments of various kinds must be done over a significant range of energies. This is the price we pay for the checks on consistency and physical reasonableness, and it is perhaps not a disadvantage in the long run, because it never hurts really to know what's going on.

References

1. E. P. Wigner and L. Eisenbud, Phys. Rev. 72, 29 (1947).

2. The most complete description is still A. M. Lane and R. G. Thomas, Rev. Mod. Phys. 30, 257 (1958).

3. References to data shown in the figures are given in the Appendix.

4. An equivalent approach in a different formalism has been used by: Barit and Sergeyev, Yadernaya Fiz. 4, 712 (1967); Soviet J. Nucl. Phys. 4, 507 (1967).

Appendix

Data References for Figures

Fig. 1. C. A. Goulding, P. Stoler, and J. D. Seagrave, Nucl. Phys. A215, 253 (1973);

F. J. Vaughn, W. L. Imhof, R. C. Johnson, and M. Walt, Phys. Rev. 118, 683 (1960);

Los Alamos Physics and Cryogenics Groups (Battat et al.), Nucl. Phys. 12, 291 (1959).

Figs. 2-4. G. L. Morgan and R. L. Walter, Phys. Rev. 168, 1114 (1968);

D. S. Cramer and L. Cranberg, Nucl. Phys. A180, 273 (1972);

John D. Seagrave, Phys. Rev. 92, 1222 (1953);

B. Hoop, Jr. and H. H. Barschall, Nucl. Phys. 83, 65 (1966);

A. Niiler, M. Drosg, J. C. Hopkins, J. D. Seagrave, and E. C. Kerr, Phys. Rev. C 4, 36 (1971);

R. E. Shamu and J. G. Jenkin, Phys. Rev. 135B, 99 (1964).

Figs. 5-6. T. H. May, R. L. Walter, and H. H. Barschall, Nucl. Phys. 45, 17 (1963);

J. R. Sawers, Jr., G. L. Morgan, L. A. Schaller, and R. L. Walter, Phys. Rev. 168, 1102 (1968);

Th. Stammbach, J. Taylor, G. Spalek, and R. L. Walter, Phys. Rev. C 2, 434 (1970);

W. B. Broste, G. S. Mutchler, J. E. Simmons, R. A. Arndt, and L. D. Roper, Phys. Rev. C 5, 761 (1972);

F. W. Büsser, F. Niebergall, G. Söhngen, and J. Christiansen, Nucl. Phys. 88, 593 (1966).

Figs. 7-8. G. Freier, E. Lampi, W. Sleator, and J. H. Williams, Phys. Rev. 75, 1345 (1949);

A. C. L. Barnard, C. M. Jones, and J. L. Weil, Nucl. Phys. 50, 604 (1964);

N. Jarmie and J. Jett, private communication;

D. Garreta, J. Sura, and A. Tarrats, Nucl. Phys. A132, 204 (1969);

L. Brown and W. Träcnslin, Nucl. Phys. A90, 334, 339 (1967);

R. I. Brown, W. Haeberli, and J. X. Saladin, Nucl. Phys. 47, 212 (1967);

P. Schwandt, T. B. Clegg, and W. Haeberli, Nucl. Phys. A163, 432 (1971);

P. W. Keaton, Jr., D. D. Armstrong, R. A. Hardekopf, F. M. Kurjan, and Y. K. Lee, Phys. Rev. Letters 29, 880 (1972).

Fig. 9. K. M. Diment, AERE-R-5224 (1967);

C. K. Bockelman, D. W. Miller, R. K. Adair, and H. H. Barschall, Phys. Rev. 84, 69 (1951).

Fig. 10. R. L. Macklin and J. H. Gibbons, Phys. Rev. 165, 1147 (1968);

E. A. Davis, F. Gabbard, T. W. Bonner, and R. Bass, Nucl. Phys. 27, 448 (1961);

M. Coates, private communication;

S. J. Friesenhan, et al., Gulf-RT-A12210 (1972);

D. O. Nellis, W. E. Tucker, and I. L. Morgan, Phys. Rev. C 1, 847 (1970).

Fig. 11. R. O. Lane, S. L. Hausladen, J. F. Monahan, A. J. Elwyn, F. P. Mooring, and A. Langsdorf, Jr., Phys. Rev. C 4, 380 (1971).

Fig. 12. L. Van der Zwaan and K. W. Geiger, Nucl. Phys. A180, 615 (1972).

Fig. 13. R. Y. Cusson, Thesis, California Institute of Technology (1965).

Fig. 14. A. Hemmendinger, Bull. APS, Series II, 1, 96 (1956);

M. Ivanovich, P. G. Young, and G. G. Ohlsen, Nucl. Phys. A110, 441 (1968);

R. J. Spiger and T. A. Tombrello, Phys. Rev. 163, 964 (1970);

P. W. Keaton, Jr., D. D. Armstrong, and L. R. Veeser, Phys. Rev. Letters 20, 1392 (1968), and private communication.

Fig. 15. R. O. Lane, A. J. Elwyn and A. Langsdorf, Jr., Phys. Rev. B 136, 1710 (1964);

J. C. Overley, R. M. Sealock, and D. H. Ehlers, Nucl. Phys. A221, 573 (1974);

H. H. Knitter and M. Coppola, EANDC (E)-57 (U) (EUR-3454) (1967).

Fig. 16. C. T. Hibdon and R. R. Weeks, ANL Physics Div. Quarterly Report (1954);

C. T. Hibdon and F. P. Mooring, Conf. on Neutron Cross Section Technology, Washington, 1968, p. 159;

G. V. Gorlov, B. M. Gokhberg, V. M. Morozov, and G. A. Otroshchenko, Doklady Akad. 111, 791 (1956); Doklady Akad. 1, 598 (1956);

J. A. Farrell, Conference on Neutron Cross Section Technology, Washington, 1968, p. 153;

C. H. Johnson, B. Willard, and J. K. Bair, Phys. Rev. 96, 985 (1954);

C. A. Goulding and P. Stoler, EANDC (US) - 176 U, p. 161 (1972);

J. W. Meadows and J. F. Whalen, Nucl. Sci. Eng. 41, 351 (1970);

S. J. Bame, Jr. and R. L. Cubitt, Phys. Rev. 114, 1580 (1959);

W. B. Pardo, J. H. Roberts, Bull. Am. Phys. Soc. 4, 218 (1959);

J. B. Weddell, J. H. Roberts, Phys. Rev. 95, 117 (1954);

M. Coates, private communication;

L. G. Stromberg, S. Schwarz, A. Bergstrom, Nucl. Phys. 63, 593 (1965);

S. A. Cox and F. R. Pontet, J. Nucl. Energy 21, 271 (1967);

W. P. Poenitz, private communication (1974);

F. Ribe, Phys. Rev. 103, 741 (1956);

R. B. Murray, H. W. Schmitt, Phys. Rev. 115, 1707 (1959).

Fig. 17. V. König, W. Grüebler, R. E. White, P. A. Schmelzbach and P. Marmier, Nucl. Phys. A185, 263 (1972).

Fig. 18. Ch. Leeman, H. Burgesser, P. Huber, V. Rohrer, H. Schieck, and F. Seiler, Helv. Phys. Acta 44, 141 (1971).

Ch. Leeman, H. Meiner, V. Rohrer, J. X. Saladin, F. Seiler, P. Huber, W. Grüebler, V. König, and P. Marmier, Polarization Phenomena in Nuclear Reactions, ed. H. H. Barschall and W. Haeberli, Univ. of Wisconsin Press, Madison (1970), p. 548;

G. G. Ohlsen and K. Mitchell, private communication;

W. Grüebler, V. König, A. Ruh, P. A. Schmelzbach, R. E. White and P. Marmier, Nucl. Phys. A165, 505 (1971).

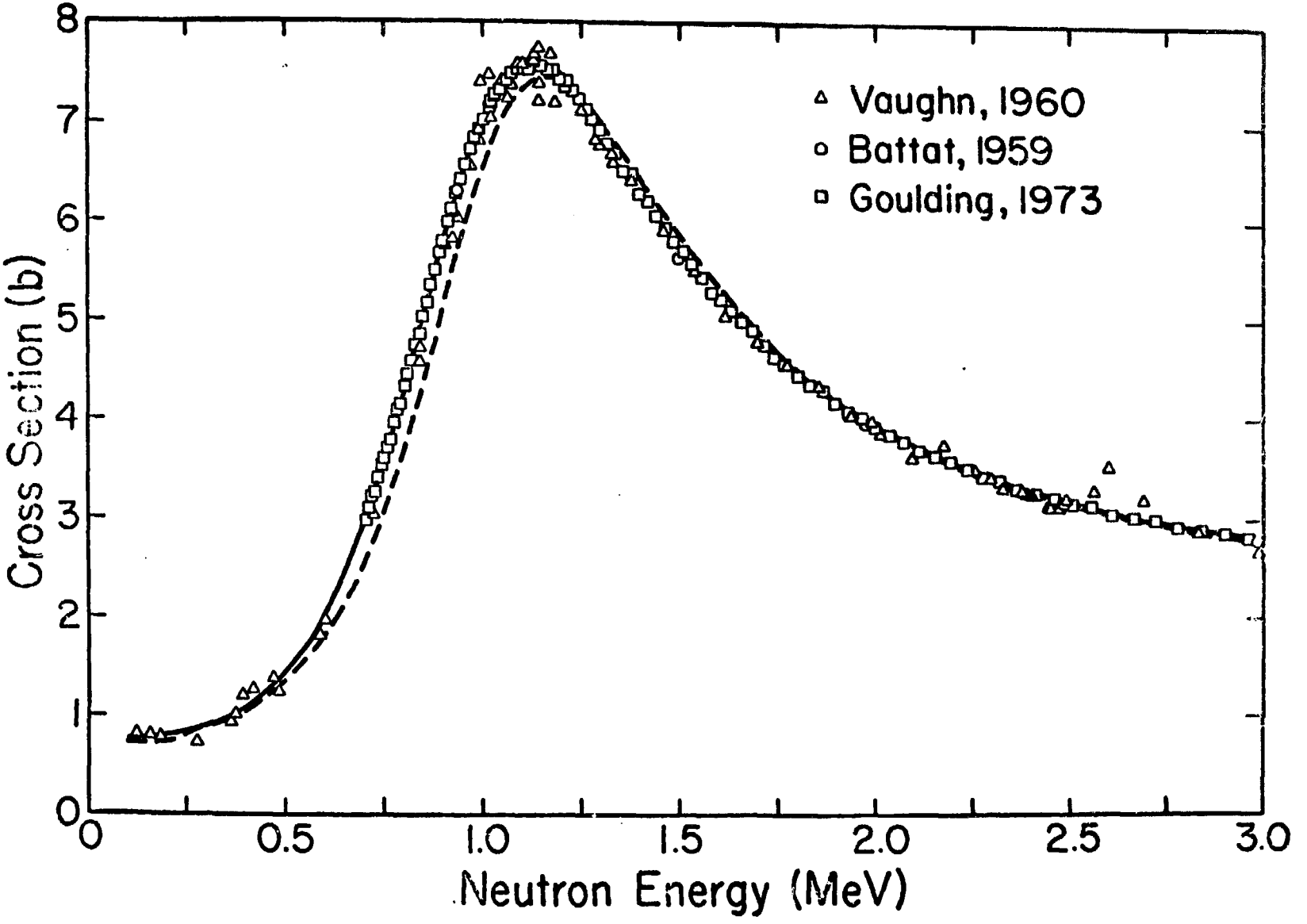

Fig. 1. Total n-^{4}He cross section, E_n = 0-3 MeV

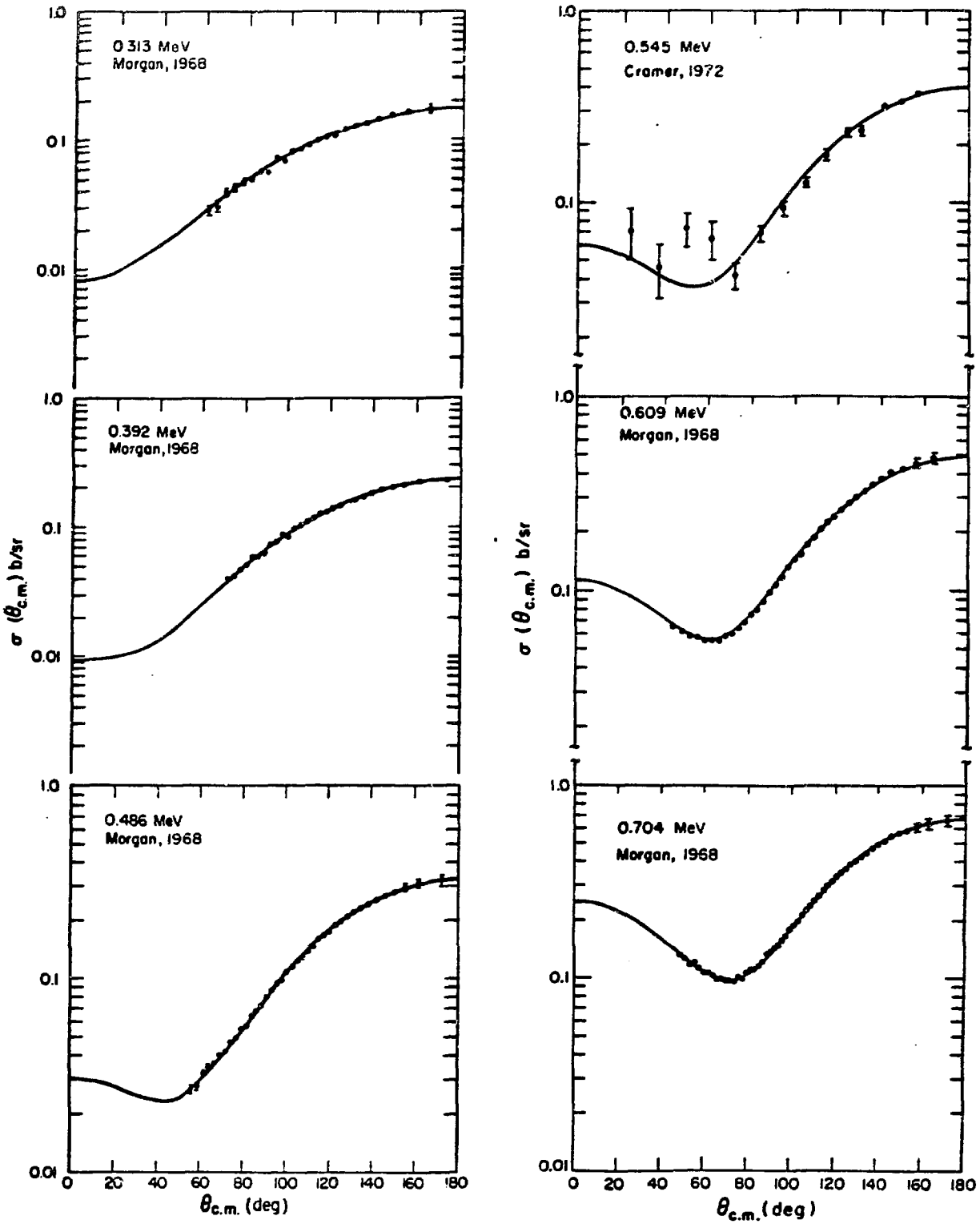

Fig. 2. $^{4}He(n,n)^{4}He$ differential cross sections, E_n = .3-.7 MeV

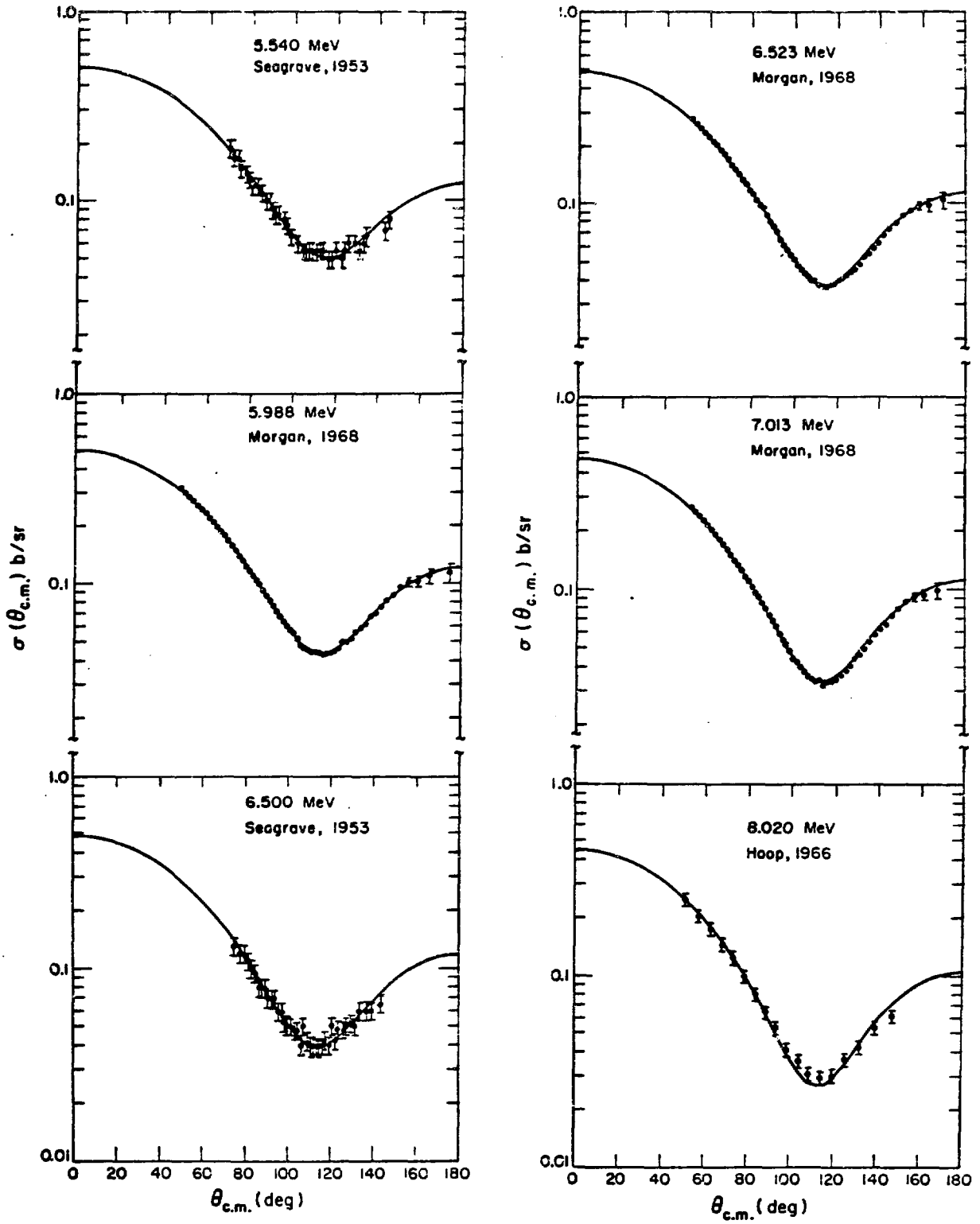

Fig. 3. $^{4}He(n,n)^{4}He$ differential cross sections, E_n = 5.5-8 MeV

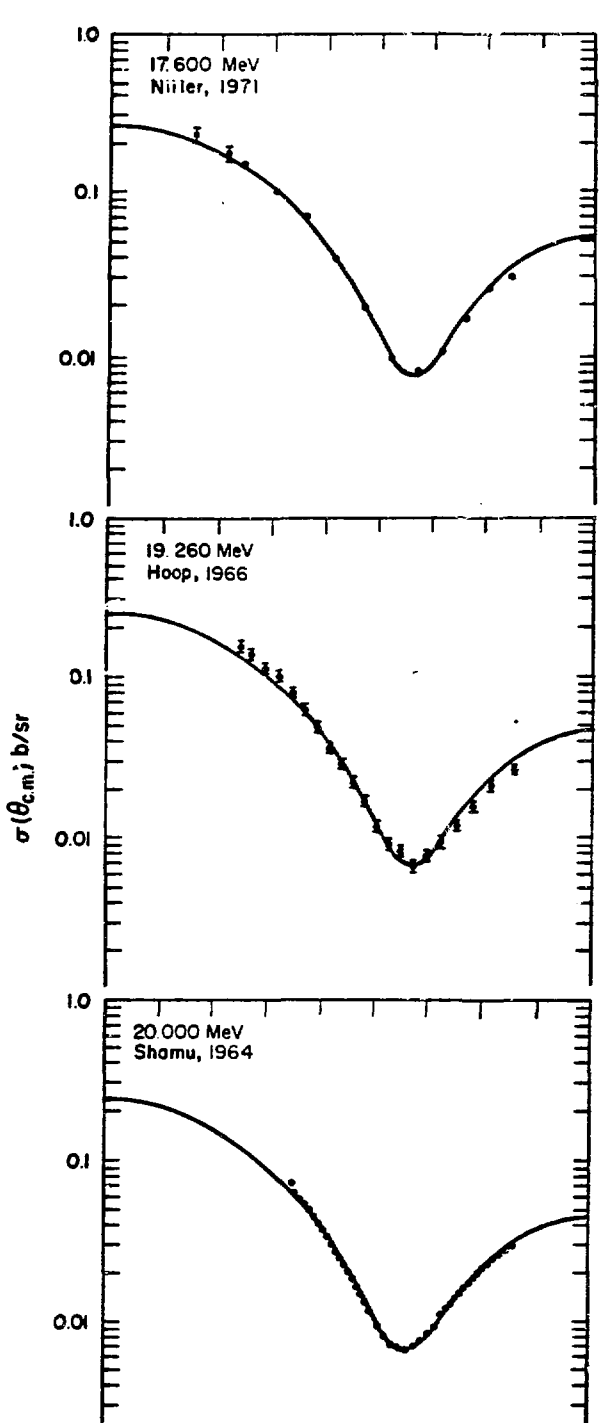

Fig. 4. $^{4}He(n,n)^{4}He$ differential cross sections, E_n = 17.6-20 MeV

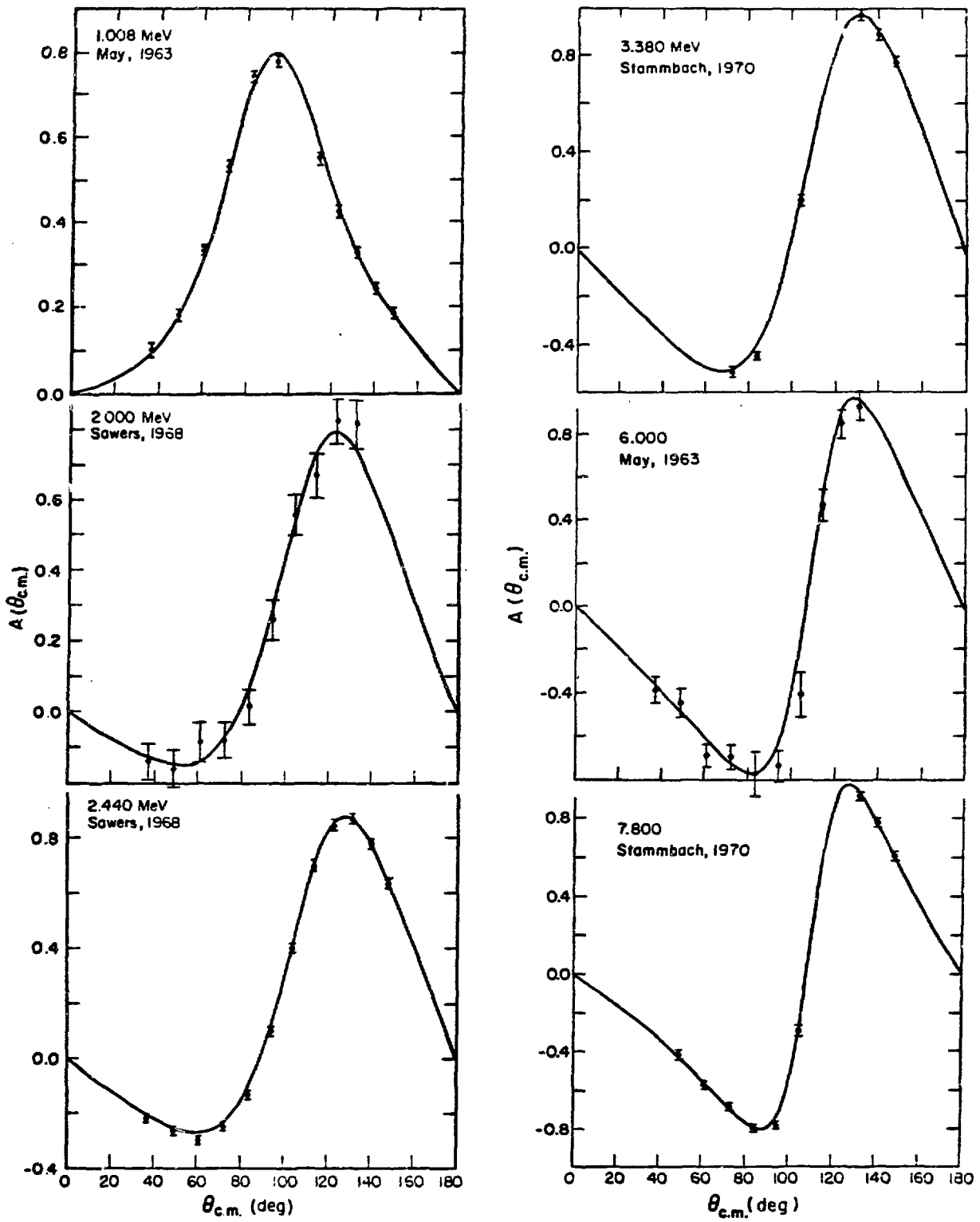

Fig. 5. $^{4}He(n,n)^{4}He$ neutron polarizations, E_n = 1-7.8 MeV

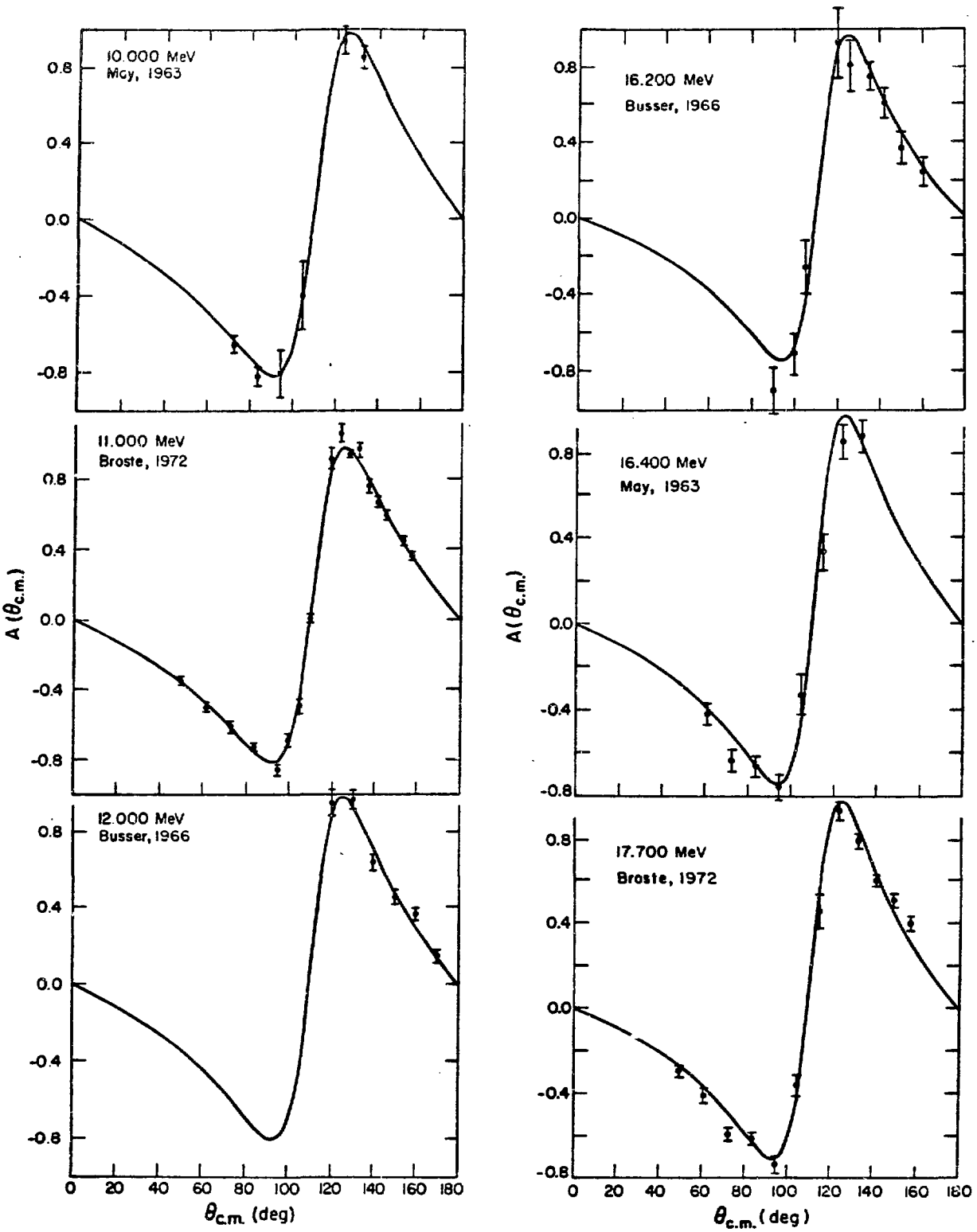

Fig. 6. $^{4}He(n,n)^{4}He$ neutron polarizations, E_n = 10-17.7 MeV

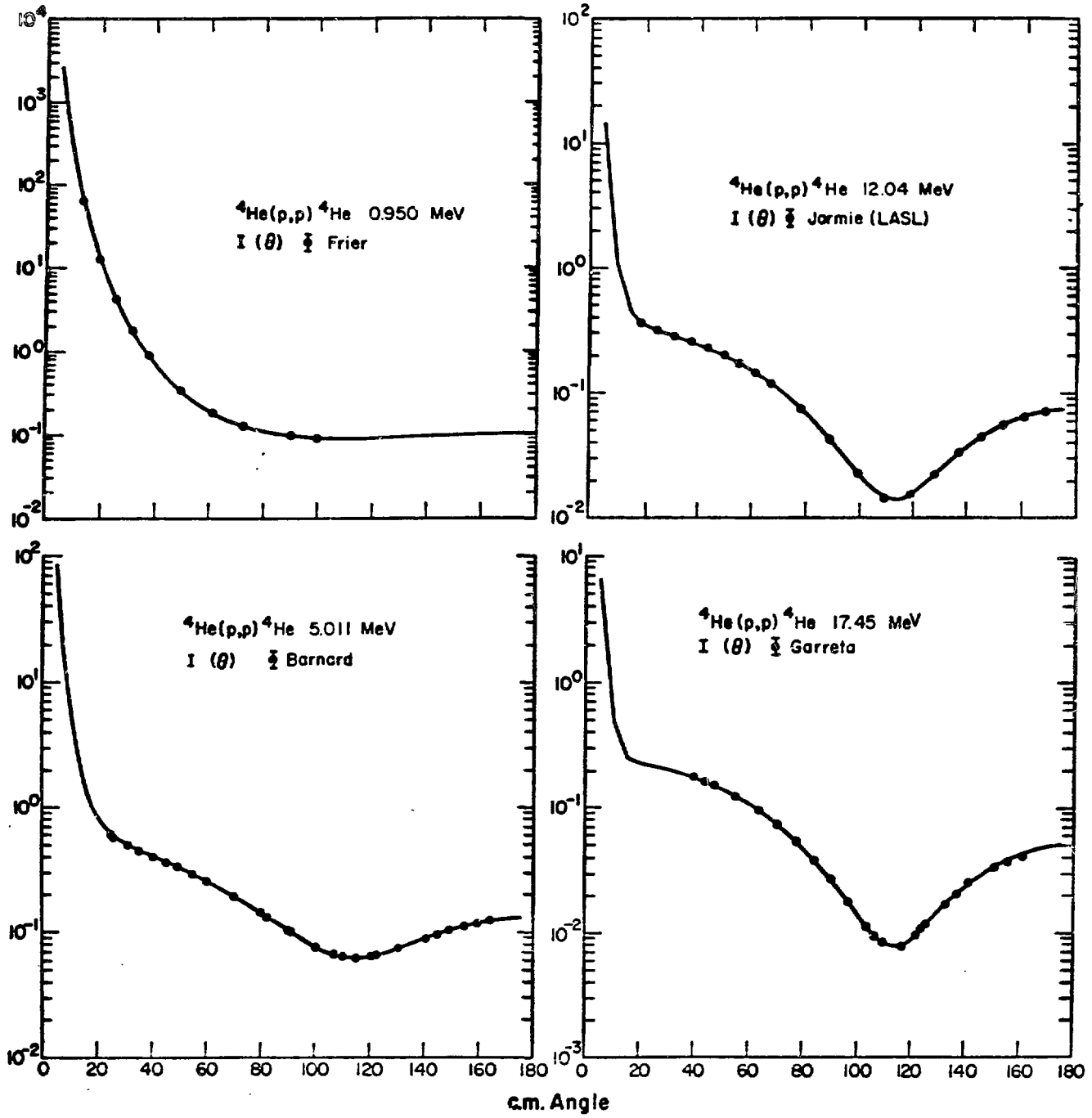

Fig. 7. ^{4}He(p,p)^{4}He differential cross sections, E_p = .95-17.5 MeV

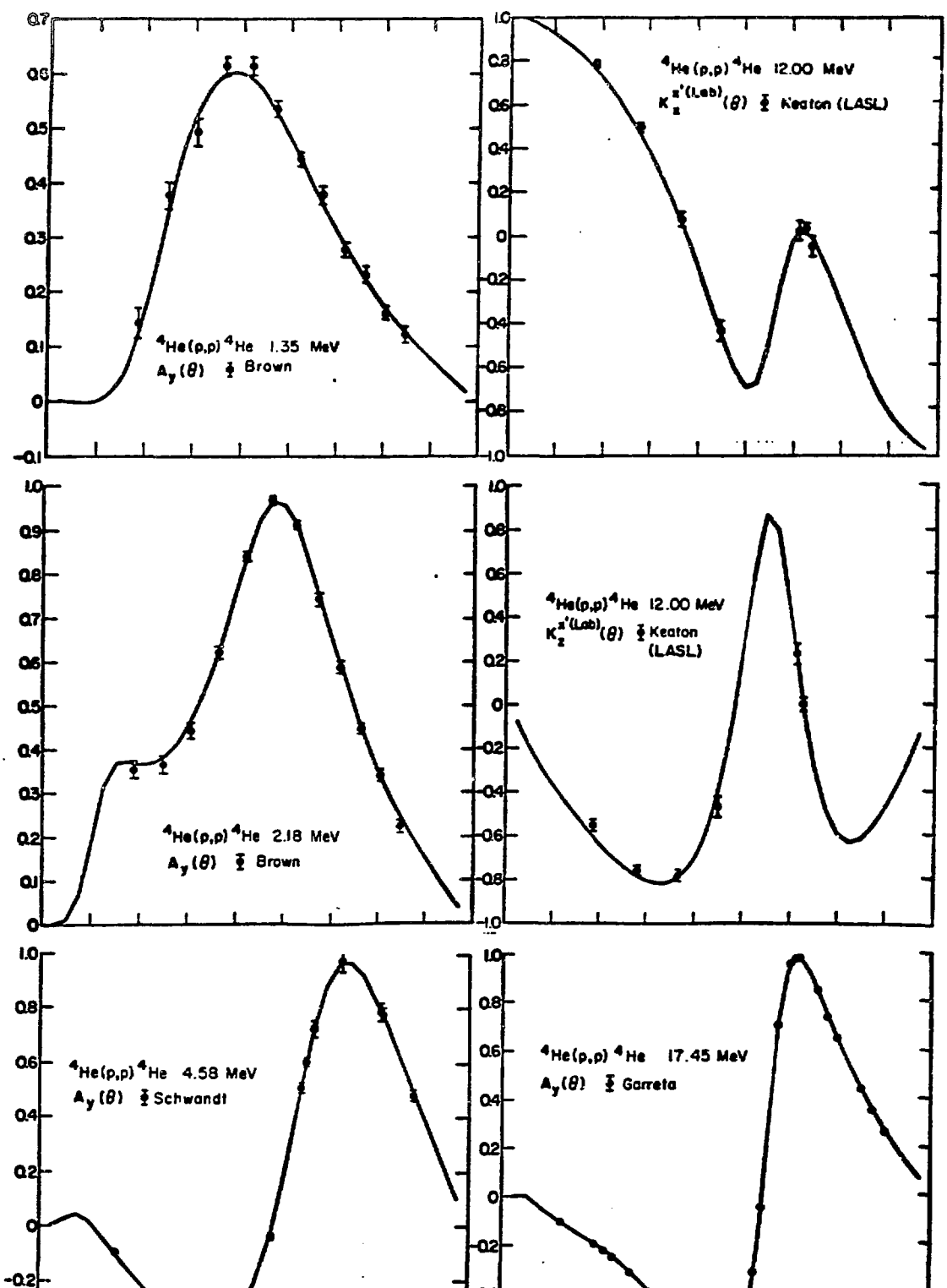

Fig. 8. ^{4}He(p,p)^{4}He proton polarizations, polarization transfers, E_p = 1.4-17.5 MeV

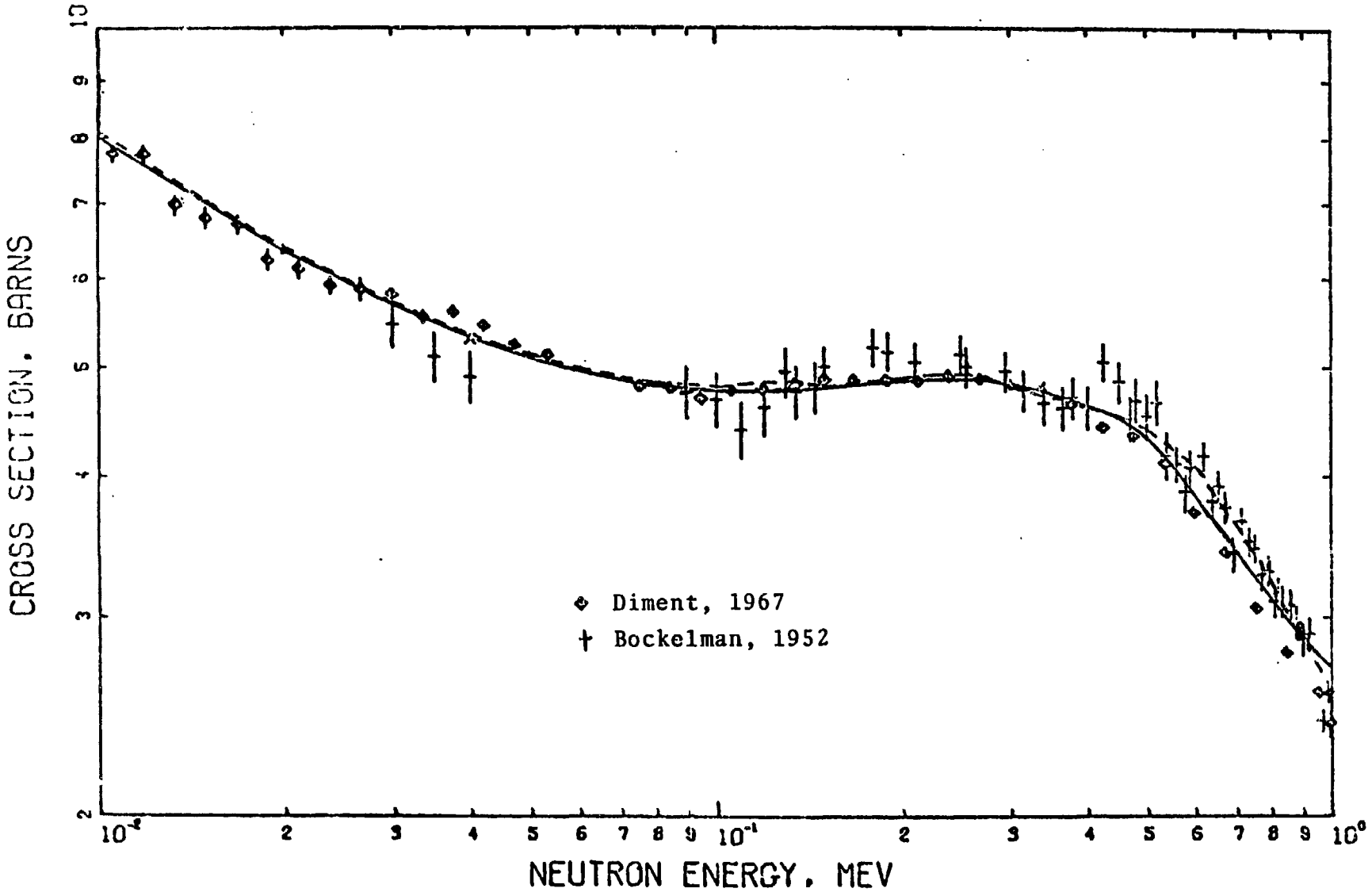

Fig. 9. Total n-^{10}B cross section, E_n = .01-1.0 MeV

^{11}B SYSTEM

Reaction	Observable Types Analyzed:			
	Total Neutron Cross Section	Integrated Cross Section	Differential Cross Section	Polarization
^{10}B	X			
$^{10}B(n,n)^{10}B$		X	X	X
$^{10}B(n,\alpha_0)^{7}Li$		X	X	
$^{10}B(n,\alpha_1)^{7}Li^*$		X	X	
$^{7}Li(\alpha,\alpha_0)^{7}Li$			X	
$^{7}Li(\alpha,\alpha_1)^{7}Li^*$		X		

Fig. 9a. Types of data included in ^{11}B analysis.

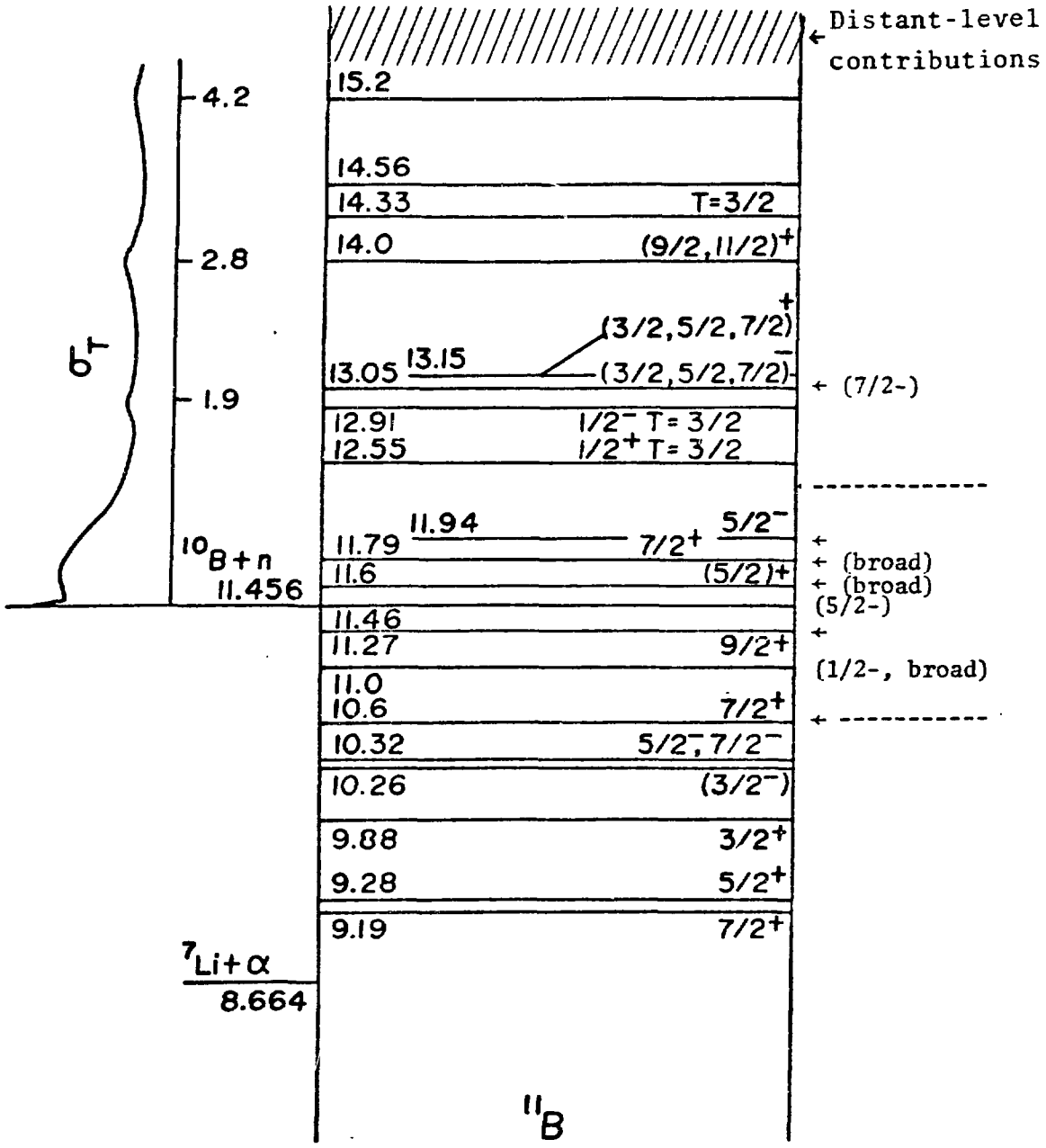

Fig. 9b. Level diagram for ^{11}B. The dotted lines indicate the range over which data were included. Checked levels correspond approximately to those in our analysis. Additional levels found in the analysis are indicated in parentheses or brackets.

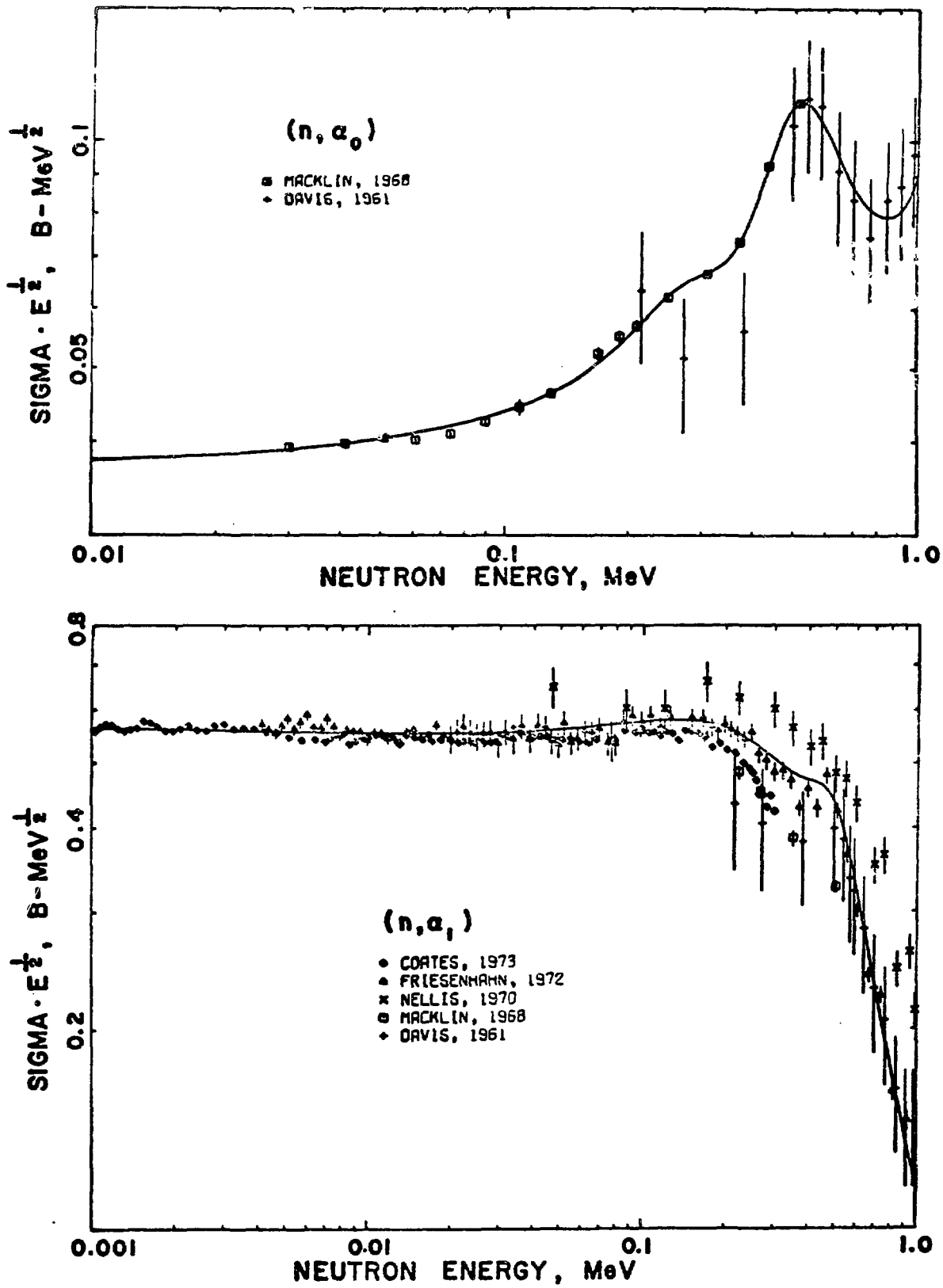

Fig. 10. Integrated $^{10}B(n,\alpha_0)^7Li$ and $^{10}B(n,\alpha_1)^7Li^*$ cross sections below E_n = 1 MeV

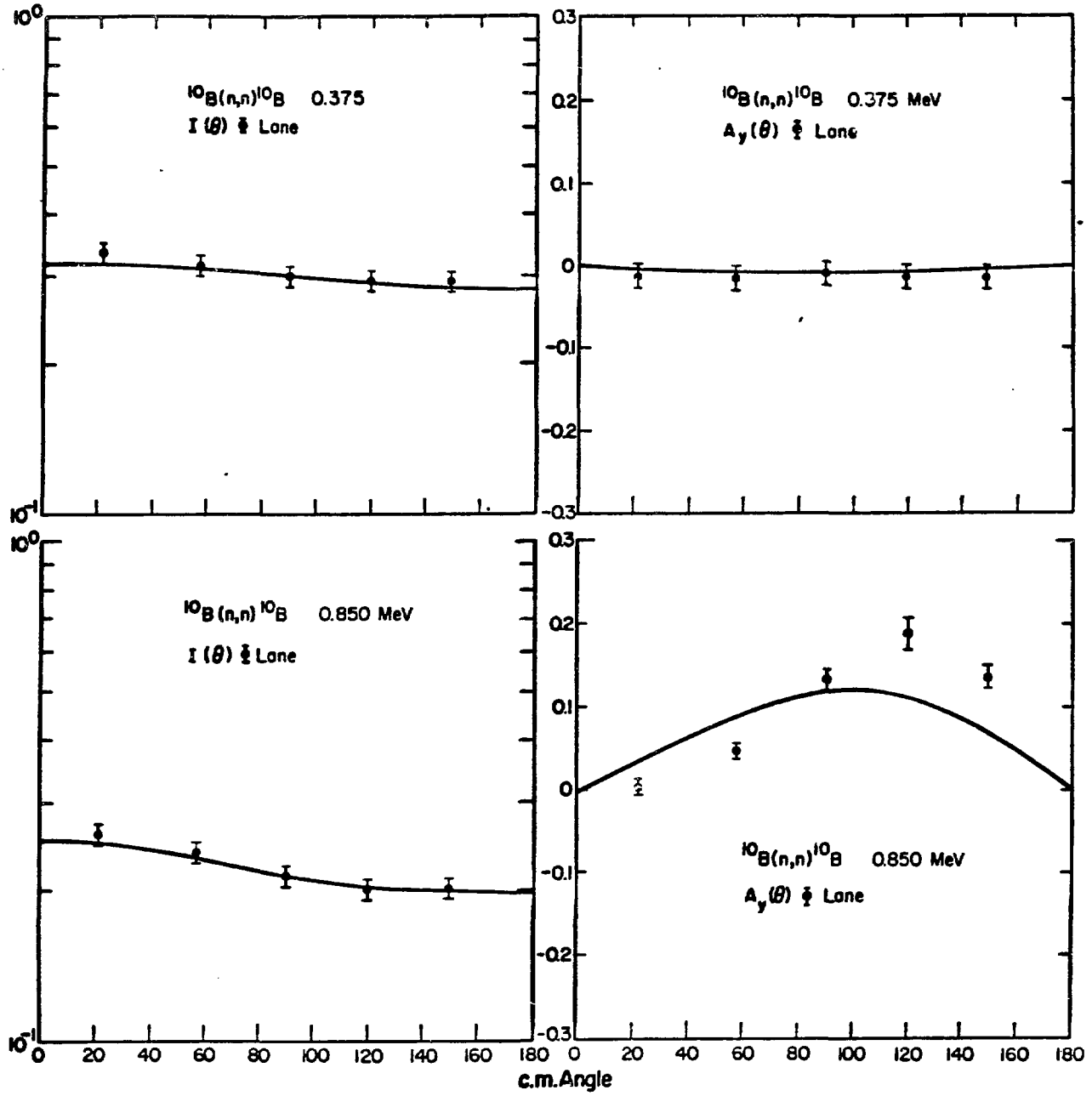

Fig. 11. $^{10}B(n,n)^{10}B$ differential cross sections and neutron polarizations at E_n = .375 and .850 MeV

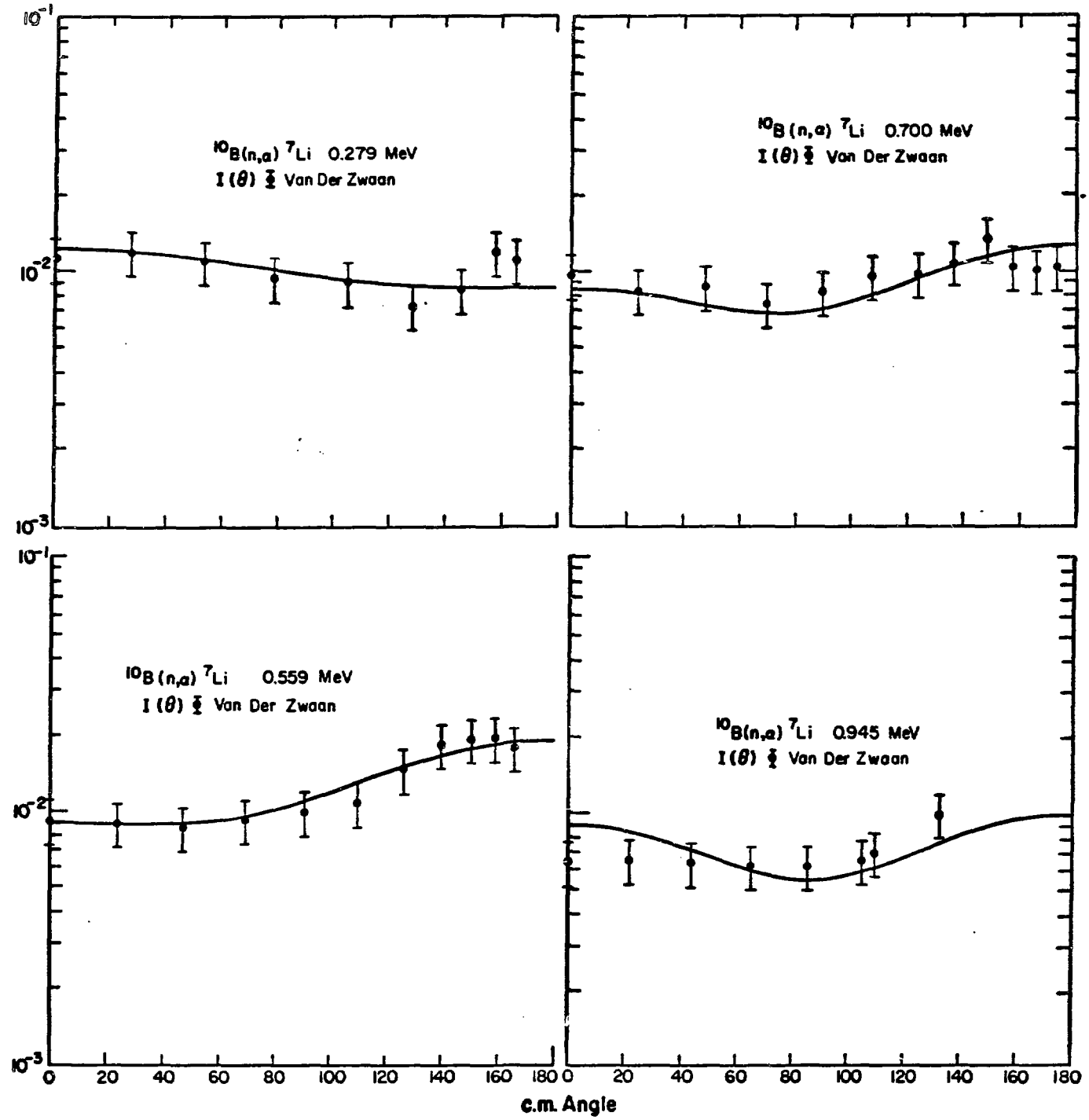

Fig. 12. $^{10}B(n,\alpha_0)^{7}Li$ differential cross sections, E_n = .28-.95 MeV

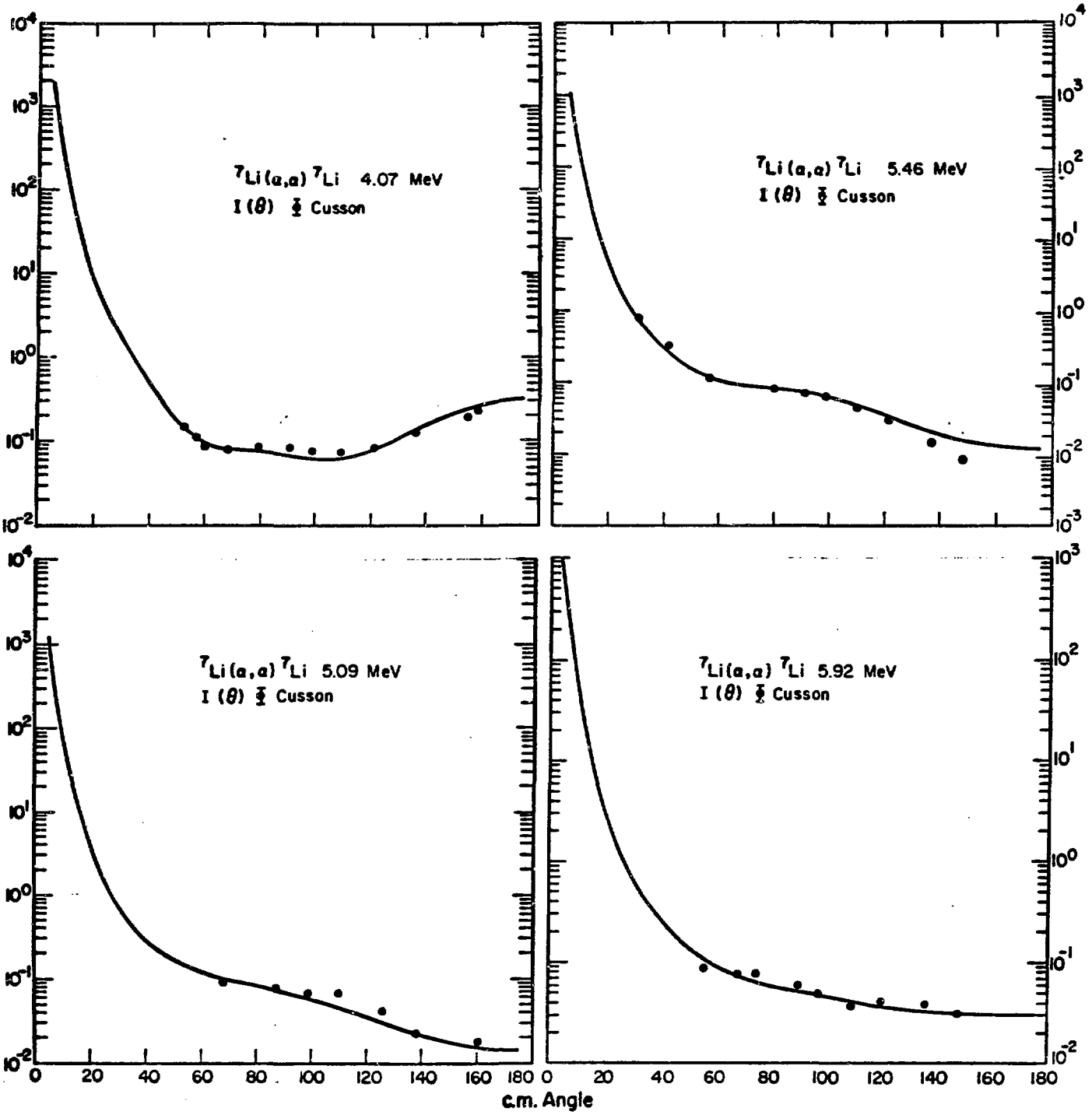

Fig. 13. ^{7}Li(α,α)^{7}Li differential cross sections, E_α = 4.1-6.92 MeV

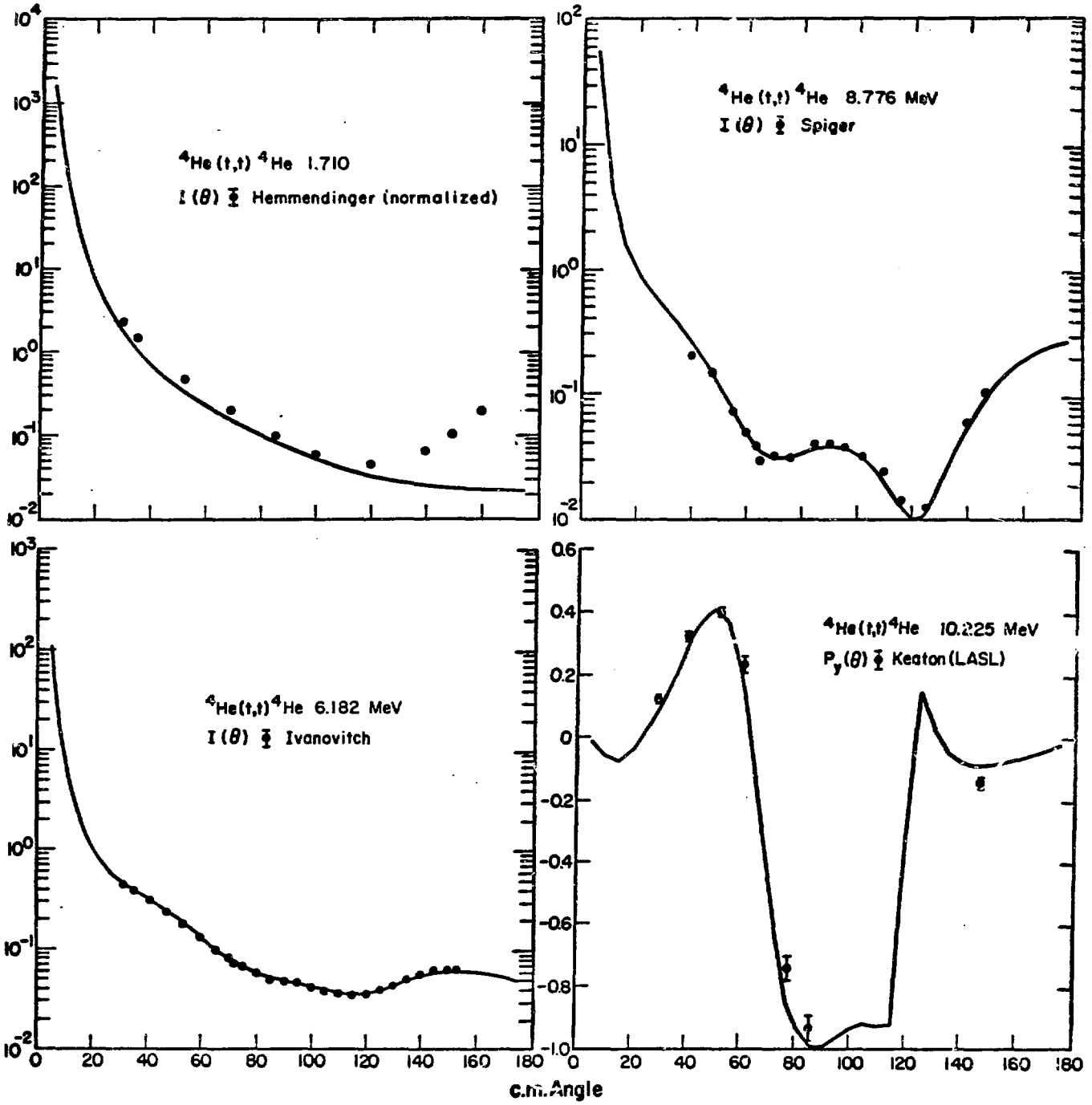

Fig. 14. ^{4}He(t,t)^{4}He differential cross sections for E_t = 1.7 to 8.8 MeV and triton polarization, E_t = 10.2 MeV

^{7}Li SYSTEM

Reaction	Observable Types Analyzed:			
	Total Neutron Cross Section	Integrated Cross Section	Differential Cross Section	Polarization
^{6}Li	X			
^{6}Li(n,n)^{6}Li		X	X	X
^{6}Li(n,α)T		X	X	
^{4}He(t,t)^{4}He			X	X

Fig. 14a. Types of data included in ^{7}Li analysis

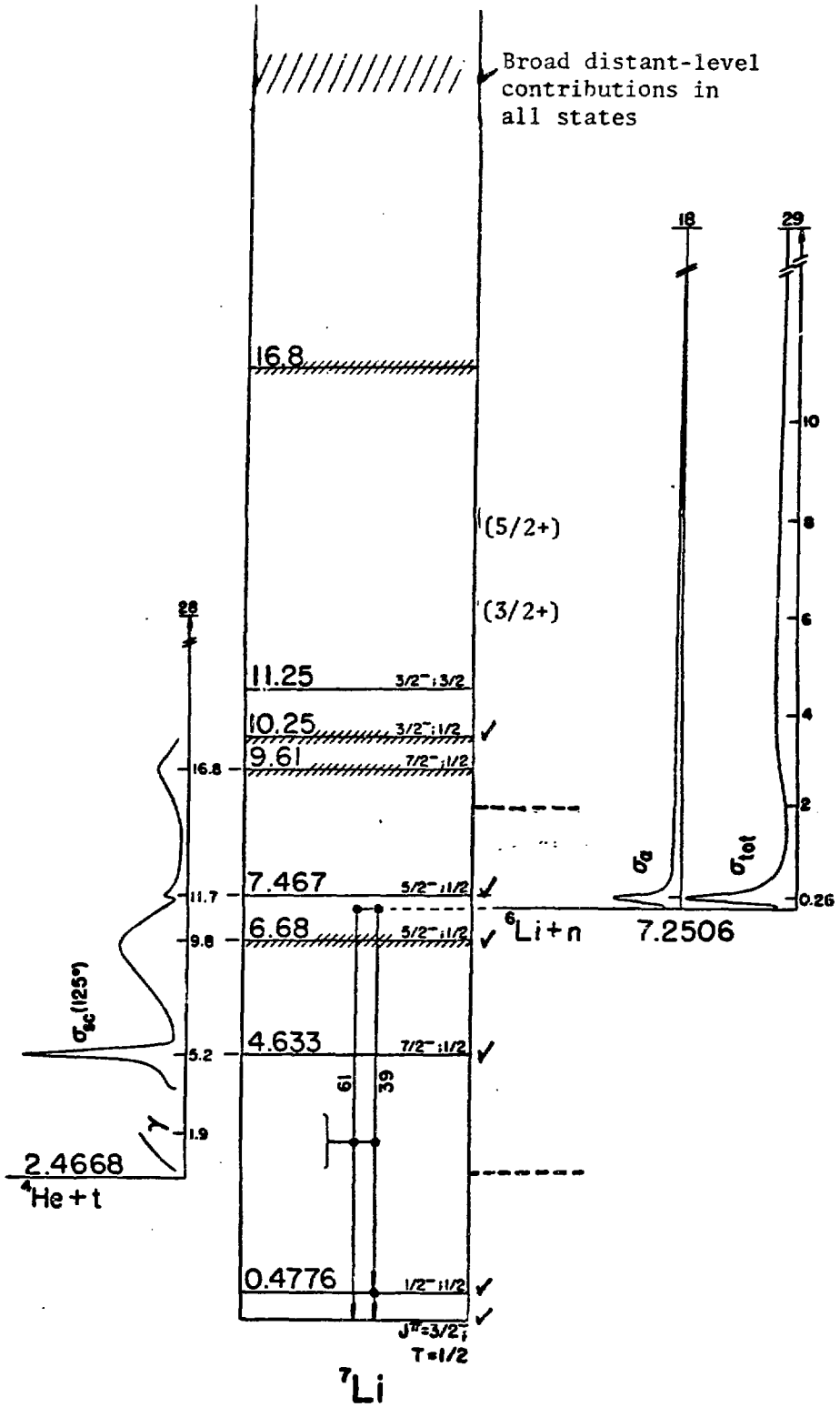

Fig. 14B. Level diagram for ^{7}Li. The dotted lines indicate the range over which data were included. Checked levels correspond approximately to those in our analysis. Additional levels found in the analysis are indicated in parentheses or brackets.

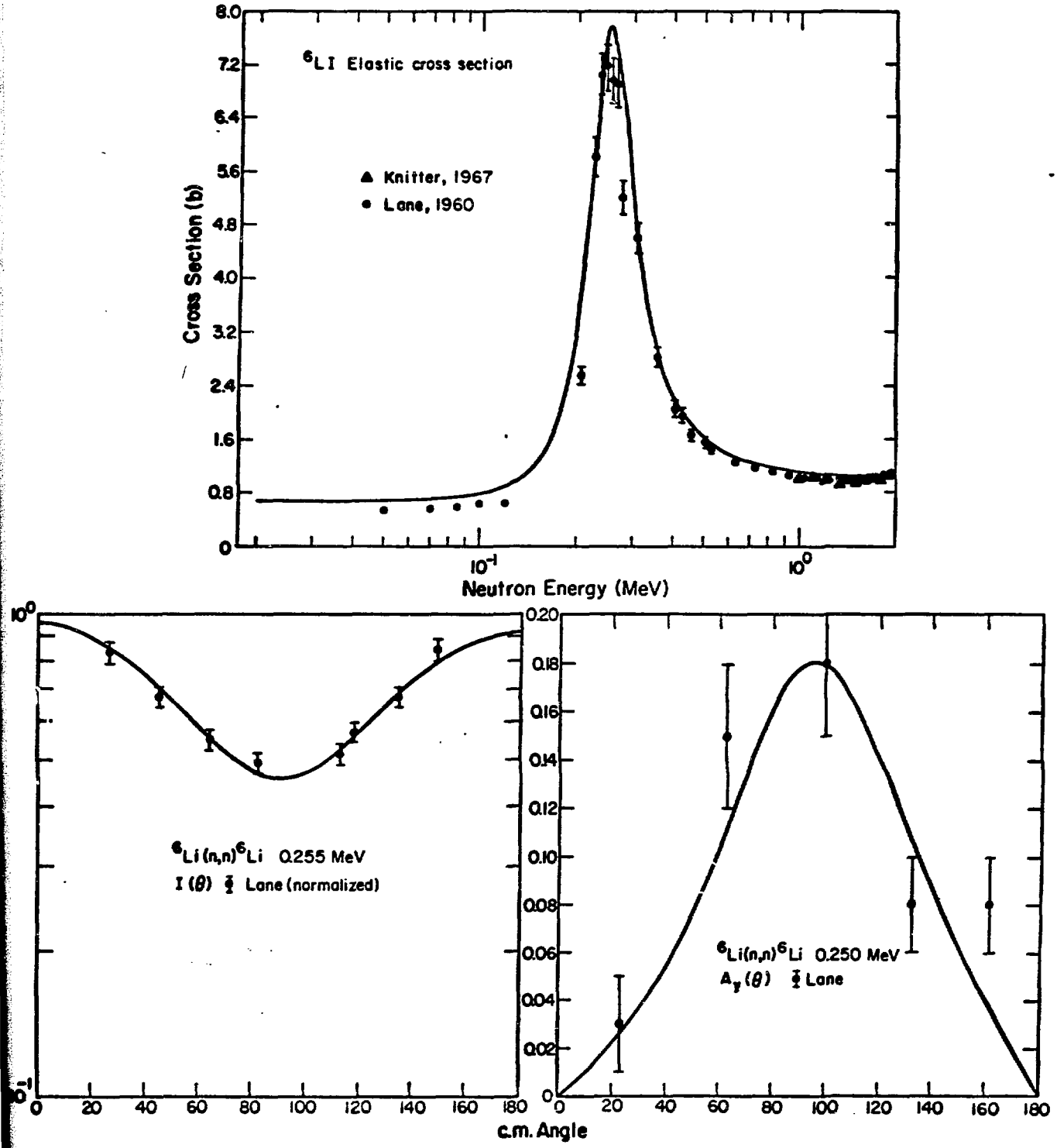

Fig. 15. ^{6}Li(n,n)^{6}Li observables near the resonance at $E_n \approx .250$ MeV

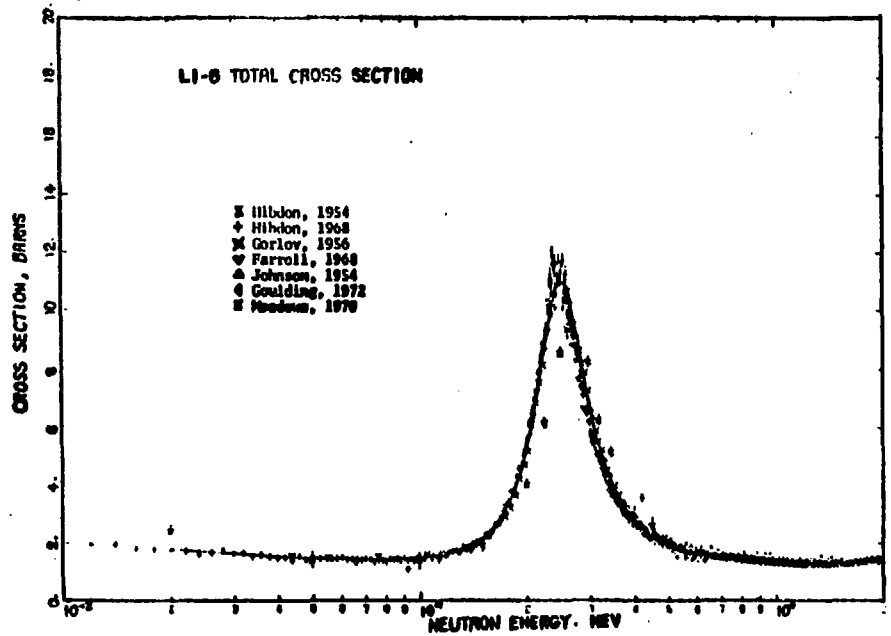

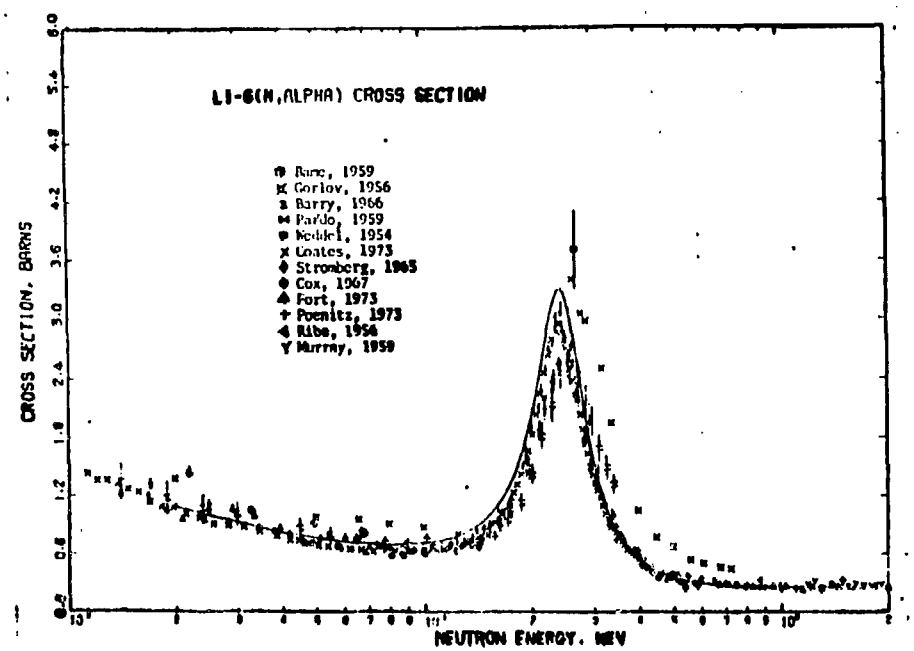

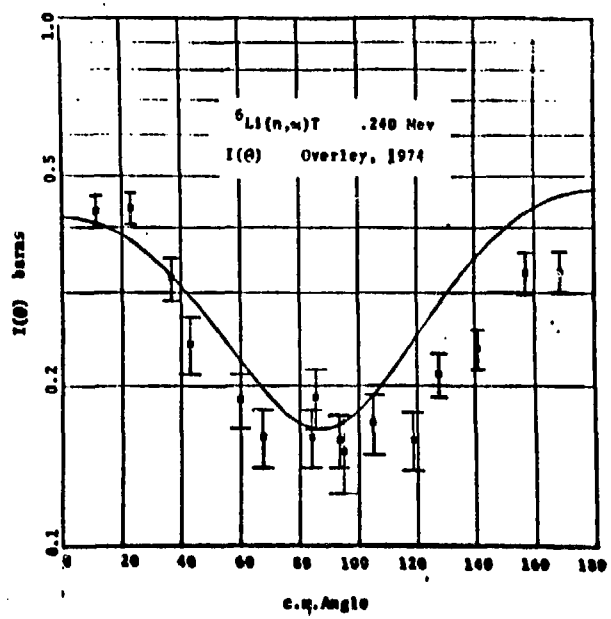

Fig. 16. n-^{6}Li total cross section, ^{6}Li(n,α)T observables near the resonance at $E_n \approx .250$ MeV

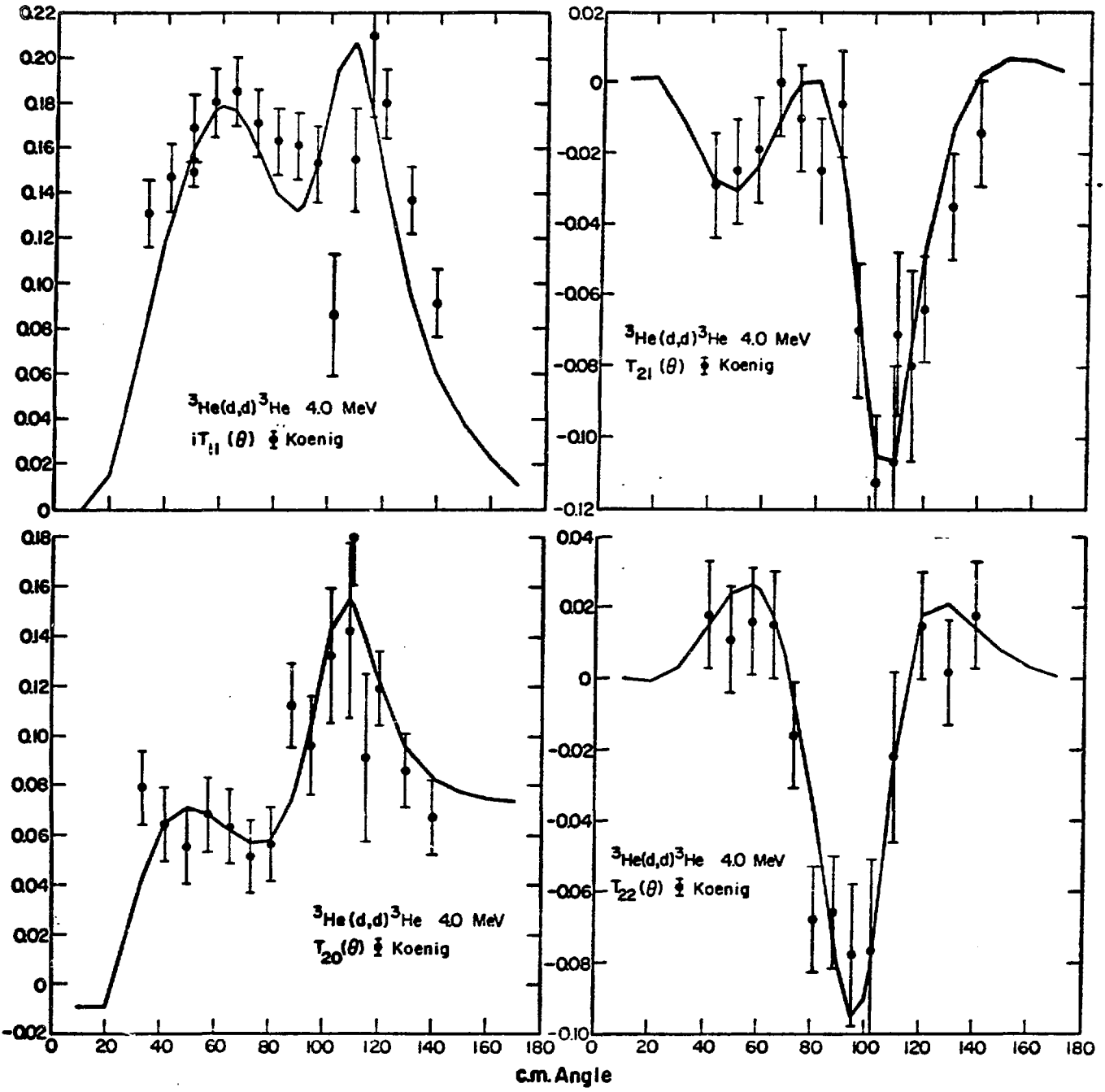

Fig. 17. ^{3}He(d,d)^{3}He deuteron analyzing tensors iT_{11}, T_{20}, T_{21}, and T_{22} at E_d = 4.0 MeV.

^{5}Li SYSTEM

Reaction	Observable Types Analyzed:				
	Integrated Cross Section	Differential Cross Section	Polarization*	Spin Correlation	Polarization Transfer
^{3}He(d,d)^{3}He		X	X	X	X
^{3}He(d,p)^{4}He	X	X	X	X	X
^{4}He(p,p)^{4}He		X	X		X

*"Polarization" heading is also meant to include analyzing power measurements made with either polarized beam or polarized target.

Fig. 17a. Types of data included in ^{5}Li analysis.

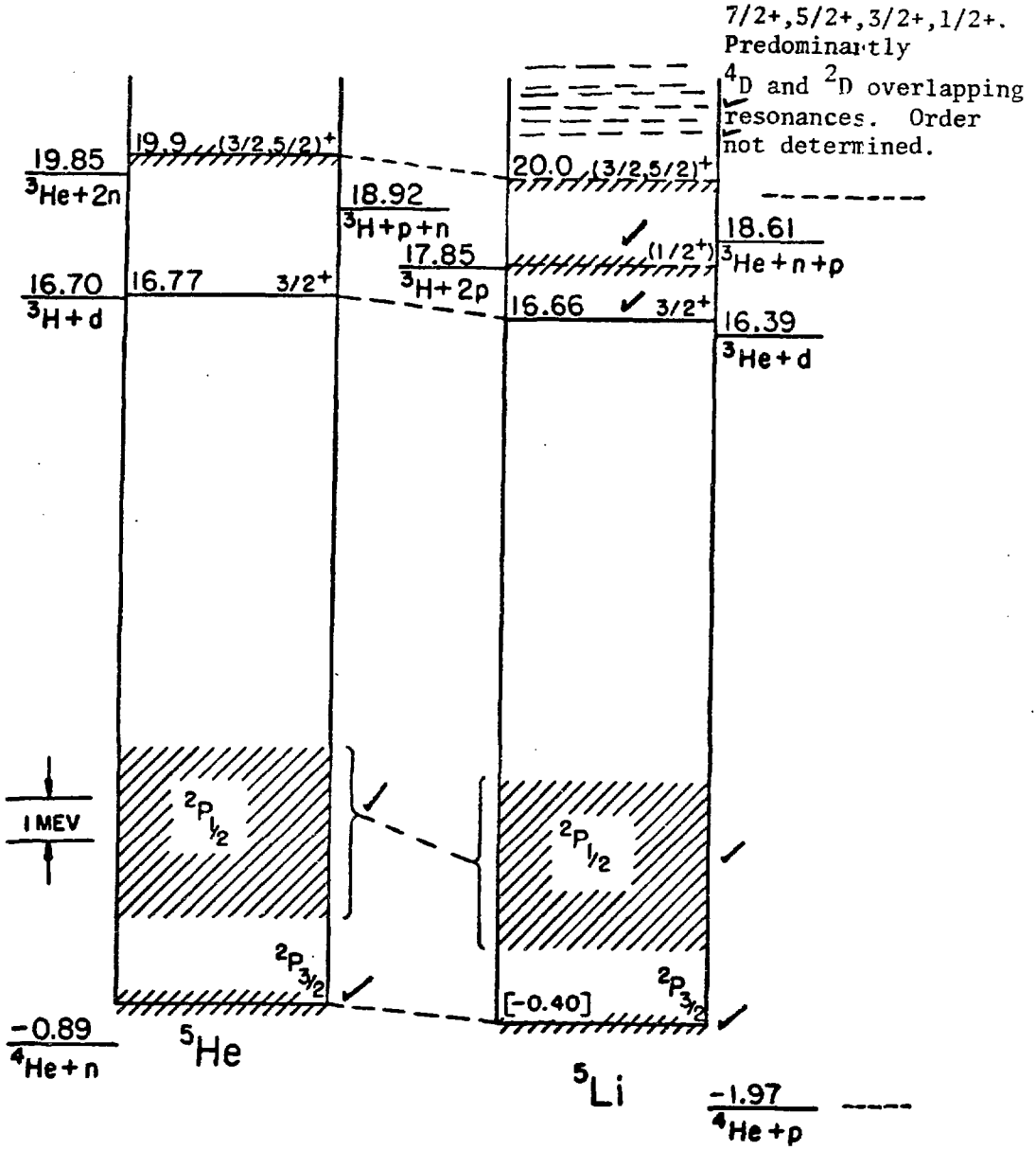

Fig. 17b. Level diagram for ^{5}He, ^{5}Li. The dotted lines indicate the range over which data were included. Checked levels correspond approximately to those in our analysis. Additional levels found in the analysis are indicated in parentheses or brackets.

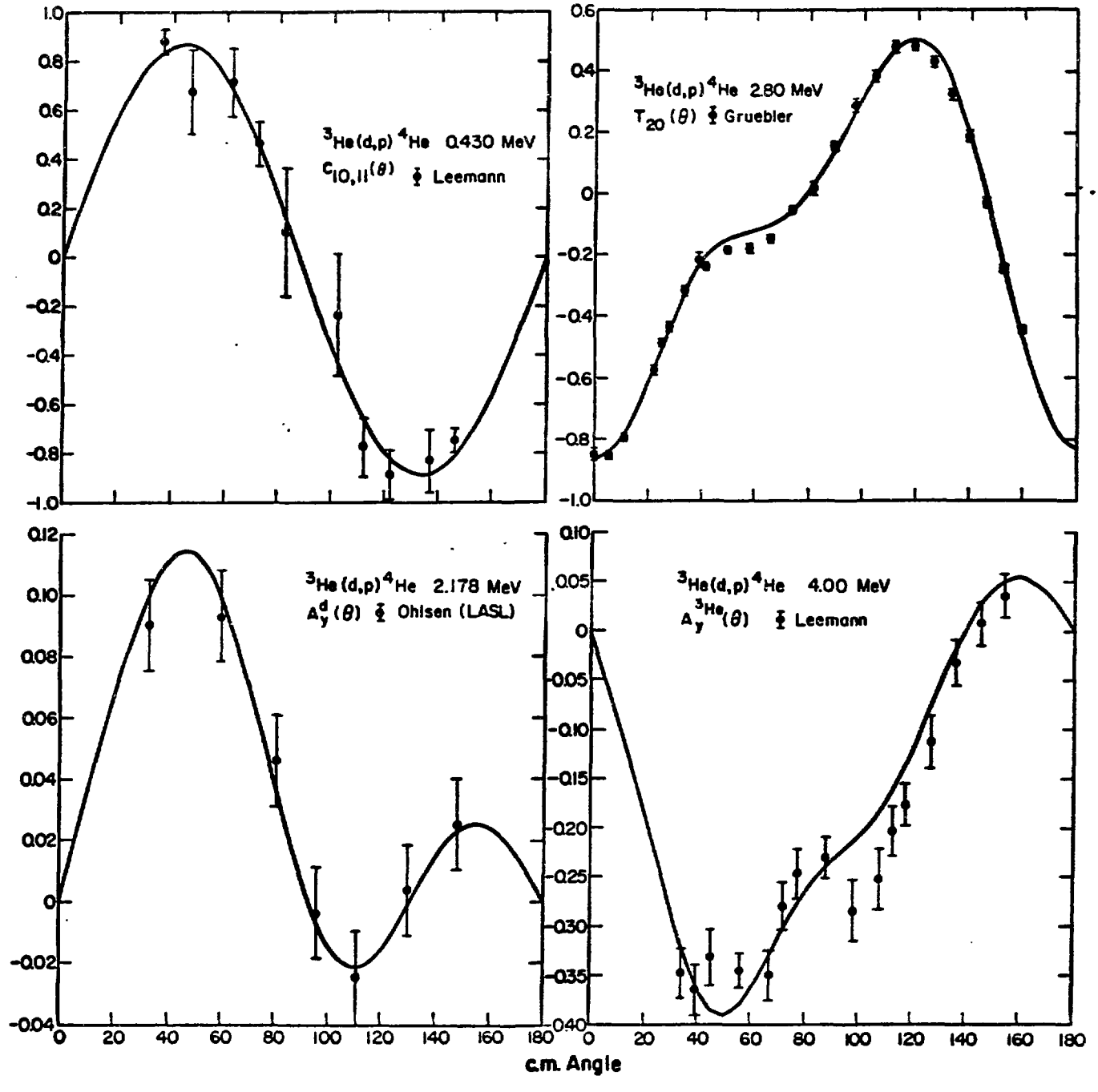

Fig. 18. ^{3}He(d,p)^{4}He measurements with polarized beams and targets, E_d = .43 - 4.0 MeV.